Int. J. Electrochem. Sci., 14 **(2019)** 717 – 725, doi: 10.20964/2019.01.05

International Journal of
ELECTROCHEMICAL
SCIENCE
www.electrochemsci.org

Short Communication

Synthesis and Electrochemical Characteristics of $LiNi_{0.5}Mn_{1.5}O_4$ Coatings Prepared by Atmospheric Plasma Spray as Cathode Material for Lithium-Ion Batteries

Xinghua Liang[1,2], *Yuchao Zhao*[*], *DiHan*[1], *Jie Mao*[2], *Lingxiao Lan*[1]

[1] Guangxi Key Laboratory of Automobile Components and Vehicle Technology, Guangxi University of Science & technology, Liuzhou 545000, China;
[2] Guangdong Institute of New Materials, National Engineering Laboratory for Modern Materials Surface, Guangdong Academy of Science, Guangzhou 510651, China
[*]E-mail: zhaoyc815@163.com

Received: 5 July 2018 / *Accepted:* 5 November 2018 / *Published:* 30 November 2018

The development of electric vehicles and portable electronic devices demands lighter and thinner batteries with appropriate rate capabilities, energy density and safety. In this work, we prepared $LiNi_{0.5}Mn_{1.5}O_4$ (LNMO) coatings as a cathode electrode for lithium-ion batteries using an atmospheric plasma spray (APS) method. The surface morphologies and structures of the coatings, as well as the powder, were characterized by scanning electron microscopy (SEM) and X-ray diffraction (XRD) analysis. The structural results show that the LNMO coatings have an ordered cubic structure (space group $P4_332$) and demonstrate better electrochemical performance at 55℃ than that at 25℃. With increasing discharge rates, the specific capacities of LNMO coatings decrease steadily. Electrochemical studies demonstrate that the LNMO coatings also have an acceptable discharge capacity (27 mAh/g) and excellent cycling stability at 55℃. These characteristics are due to the fact that the atmospheric plasma spray method can provide the cathode electrode with a cubic spinel structure and good electrochemical performance for lithium-ion batteries.

Keywords: atmospheric plasma spray; $LiNi_{0.5}Mn_{1.5}O_4$; coatings; lithium-ion batteries

1. INTRODUCTION

The development of lithium-ion batteries (LIBs) is of considerable importance in the face of increasing energy consumption. LIBs have been widely used in portable devices, EV, HEV, grid energy storage, etc. For several decades, LIBs have been studied for their advantages, such as high energy density, high operating voltage, safety, environment compatibility and low cost[1]. Studies have been carried out with other cathode electrodes such as lithium cobalt oxide ($LiCoO_2$)[2], lithium nickel

cobalt manganate[$Li(NiCoMn)O_2$][3], nickel cobalt lithium aluminate [$Li(NiCoAl)O_2$] and lithium iron phosphate ($LiFePO_4$)[4,5]. Lithium nickel manganese oxide ($LiNi_{0.5}Mn_{1.5}O_4$) has been extensively studied as a cathode electrode for lithium-ion batteries. It has good performance, higher energy density, high voltage, high potential, low price and high safety, and it is environmentally friendly and non-toxic[6].

However, the main disadvantages of LNMO are related to the difficulty in the preparing it by conventional solid-state reactions and its interaction with the electrolyte at high voltage, which leads to corrosion reactions and electrolyte degradation. LNMO has usually been prepared by a physicochemical process, such as high-temperature solid-state[7], sol-gel[8,9], co-precipitation[10,11], hydrothermal synthesis[12], and molten salt method[13], to obtain a product with high purity and good electrochemical performance. LNMO is a cubic spinel structure with either an ordered cubic structure (space group $P4_332$) or a disordered one (space group *Fd*-3*m*), thereby resulting in different capacities and discharge rates[14].

Traditional manufacturing processes for the preparation of the cathode plate for lithium-ion batteries are very complicated and expensive, such as roller coating, drying, pressing and other production processes, which reduce production efficiency. However, the fabrication of composite cathode electrodes by a binder-free deposition method and deposition methods such as APS are more efficient, making it is easier to fabricate LNMO coatings because these processes tend to sputter molten oxide compounds on the target body. This sputtering enables precise control of the thickness and a high deposition rate. As a consequence, grain refinement and enhancement of the density result in coatings with a higher physical strength using APS.

In this paper, we have synthesized spinel LNMO cathode powder employing a sol-gel auto-combustion method. We describe the fabrication of LNMO coatings as a cathode electrode material for Li-ion batteries by the APS method. The electrochemical properties of specimens prepared by the atmospheric plasma spray of LNMO are discussed in detail.

2. EXPERIMENT

2.1 Synthesis of $LiNi_{0.5}Mn_{1.5}O_4$

The $LiNi_{0.5}Mn_{1.5}O_4$ powder was prepared by a sol-gel auto-combustion method. Stoichiometric amounts of $LiOH{\cdot}H_2O$ (purity 90%), $Mn(CH_3COO)_2{\cdot}4H_2O$ (purity 99%), $Ni(CH_3COO)_2{\cdot}4H_2O$ (purity 98%) were dissolved in de-ionized water and stirred. A citric acid solution (the mole ratio of citric acid and all metal ions was 1:1) was added slowly and stirred continuously. The mixture was then heated to 353 K, evaporating the solvent until it was viscous. The semi-dry gel was placed in a vacuum oven at 393 K for 12 h, and an emerald transparent gel was obtained. The gel was then pre-sintered at 723 K in air to decompose the organic constituents. The obtained precursor was re-calcined at high temperature; specifically, the precursor was sintered at 723 K for 6 h, followed by an annealing treatment at 1123 K for 18 h in air.

2.2 Fabrication of $LiNi_{0.5}Mn_{1.5}O_4$ coatings and electrochemical test cells

Fig. 1 shows a schematic of the atmospheric plasma spray system used for this work, consisting of a nozzle, gas supply, control equipment, air compressor, power, water, water cycle, powder feeder and substrate. The coatings were spray-deposited on the preheated aluminium substrates by APS(MF-P1000, GTV, Germany) with a F6 plasma gun (Table 1). The LNMO coatings were annealed at 1123 K for 3 h.

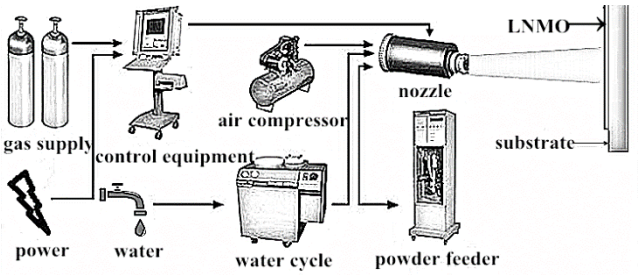

Figure 1. Schematic of the atmospheric plasma spray equipment used to deposit coatings

Table 1. Parameters of APS for LNMO coatings

Item	Gas	Value
Ar/$\times10^{-3}m^3\cdot min^{-1}$	Ar	35-42
$H_2/\times10^{-3}m^3\cdot min^{-1}$	H_2	10-12
Current/A		400
Voltage/V		60
Spray distance/mm		120
Gun moving velocity/mm • s^{-1}		450
Feed rate/$\times10^{-3}m^3\cdot min^{-1}$		1.0

The LNMO was sprayed onto the aluminium foil, which was used as a positive electrode, and lithium metal was used as a negative electrode. The two electrodes were separated by a Celgard polypropylene membrane a wand assembled into a coin-type cells (CR2016). The electrolyte employed was a solution of 1 M $LiPF_6$ in a mixture of EC/DMC with 1:1 vol ratio. The assembly of coin cells were then investigated.

2.3 Material and electrochemical characterization

The surface morphology of the coatings was investigated by scanning electron microscopy (SEM, Quanta 200, FEI, Holland) equipped with energy dispersive spectroscopy (EDS, Oxford INCAX-sight 6427). X-ray diffraction (XRD, Bruker D8 Advance) with a Cu target was used to analyse the phase purity and crystal structure of the prepared coatings. The X-ray detector was scanned in a diffraction angle range of 10 to 80 º at a speed of 2 º min^{-1}. The charge/discharge tests were carried

out using a CR2016 coin-type cell, which consisted of a LNMO-coated cathode and lithium metal anode separated by a Celgard 2400 porous polypropylene coating. Cyclic voltammetry (CV) was used to scan within the potential range of 2.5-4.5 V at a sweep rate of 0.1 mV/s.

3. RESULTS AND DISCUSSION

3.1 Microstructure of the $LiNi_{0.5}Mn_{1.5}O_4$ thin coatings

The LNMO powder and LNMO coatings X-ray diffraction data are shown in Fig. 2. Amorphous phases commonly appear during the preparation of the APS coatings[15,16]; nevertheless, the impure phases of the LNMO coatings disappear after heat treatment. The sharp diffraction peaks suggest that highly crystalline LNMO was formed. Due to the possible ordered superstructure at 2Θ =18, 37, 39, 44, 47, 57, 65 and 68[17], it is an indication that the LNMO coatings have adopted the ordered cubic structure (space group $P4_332$). The cubic lattice parameters of the annealed and un-annealed samples have been calculated from the diffraction data. The lattice constant of the samples is estimated to be a_0=0.8176 nm and 0.8178 nm, which are close to a reference value of 0.8166 nm for cubic spinel $LiNi_{0.5}Mn_{1.5}O_4$ with $P4_332$ symmetry[18].

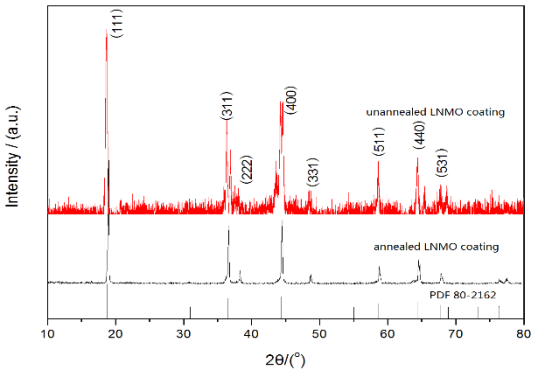

Figure 2. XRD patterns of $LiNi_{0.5}Mn_{1.5}O_4$ with and without the annealing treatment

Morphological photographs have been taken by scanning electron microscopy as shown in Fig. 3. As the SEM image shows in Fig. 3a, the diameter of the oxide polyhedrons was found to be in a range of 0.2-0.8 μm, which is smaller and more uniform than that of the annealed LNMO surface coatings. The results show that the narrow distribution of small particles can shorten the Li+ diffusion path and improve the charge-discharge performance of the electrode[19]. The annealed LNMO coatings exhibited well crystallized grains with an average size of approximately 1-4 μm (Fig. 3b). Surface particle size distribution determined that the particles in the LNMO coatings are larger than powder.

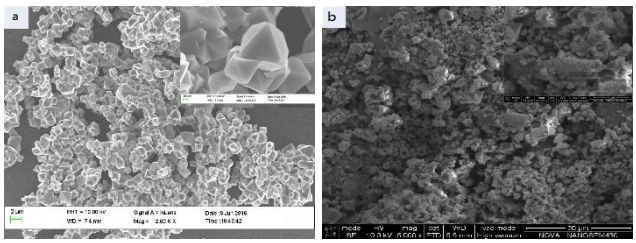

Figure 3. SEM images of $LiNi_{0.5}Mn_{1.5}O_4$ powder (a), surface (b) of annealed $LiNi_{0.5}Mn_{1.5}O_4$ coatings

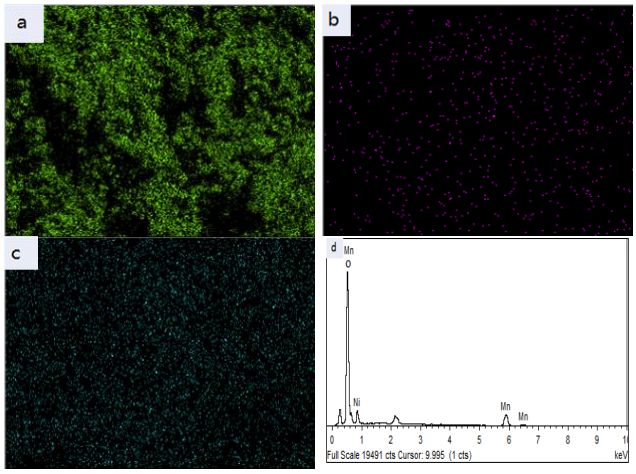

Figure 4. (a) of O, (b) of Ni, (c) of Mn, (d) EDS images of annealed $LiNi_{0.5}Mn_{1.5}O_4$ coatings

As the EDS images show in Fig. 4, O, Mn and Ni are uniform in the LNMO coatings.

3.2 Evaluation of the electrochemical properties of the $LiNi_{0.5}Mn_{1.5}O_4$ thin coatings

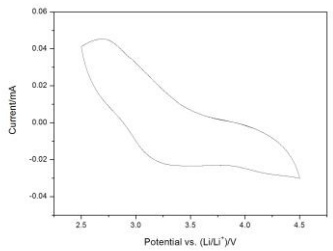

Figure 5. Cyclic voltammetry of annealed LNMO coatings electrode

The LNMO was sprayed onto the aluminium foil as cathode material for a lithium-ion battery, and the electrochemical properties are discussed. Fig. 5 shows the cyclic voltammetry (CV) of LNMO, recorded between 2.5 and 4.5 V at a scan rate of 0.1 mV s^{-1}. The cathode exhibited small redox peaks, which are attributable to Mn^{3+}/Mn^{4+} redox, near 3.25V. This outcome is well observed in typical spinel LNMO cathodes[20].

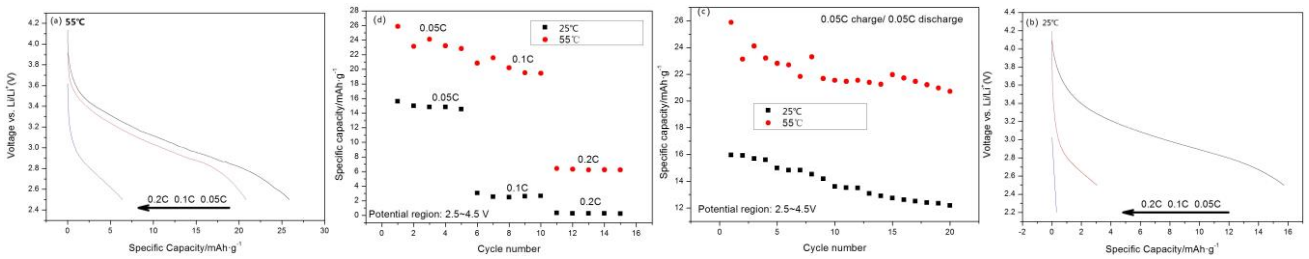

Figure 6. (a) discharge curves of annealed LNMO coating at various rates (55℃), (b) discharge curves of annealed LNMO coating at various rates (25℃), (c) cycling performance of annealed LNMO coating at 55℃ and 25℃, (d) cycling performance of annealed LNMO coating at various rates(55℃ and 25℃)

To obtain an overall evaluation of the electrochemical performance of annealed LNMO coated cathodes, the discharge performances were also tested by employing different rates of current density at 55℃ and room temperature (25℃), shown in Figs. 6(a,b). At 0.05, 0.1, and 0.2 C, the discharge capacities of LNMO coatings are 25.8, 20.9, and 6.4 $mAhg^{-1}$ at 55℃ and 15.6, 3.1, and 0.3 $mAhg^{-1}$ at 25℃, respectively. With increasing discharge rates, the specific capacities decrease steadily. Fig. 6(c) presents galvanostatic charge-discharge curves of the tested cells at 55℃ and 25℃, measured between 2.5 V and 4.5 V at a rate of 0.05 C. The figure shows that the cycle performance at 55℃ is better than that at 55℃. One possible reason is that the activity of the LNMO coated positive electrode at 55℃ is better than that at 55℃. Fig. 6(d) shows the rate performance of annealed LNMO coatings conducted from 0.05 C, 0.1 C and 0.2 C at 55℃ and 25℃. As clearly seen in Fig. 5(d), LNMO coatings have better rate performance at 55℃. It is obvious that LNMO coatings prepared by APS have better cycle performance and rate performance at 55℃ than that at 25℃.

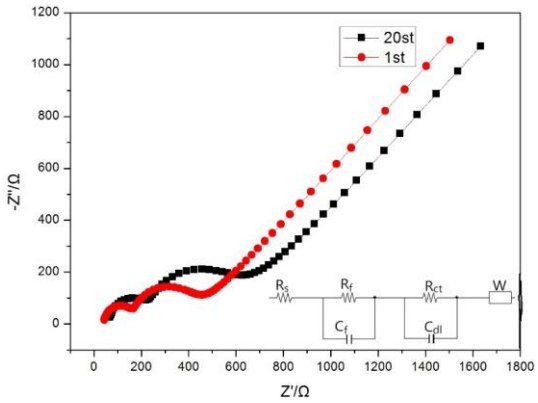

Figure 7. Electrochemical impedance spectroscopy (EIS) of annealed LNMO coatings

The electrochemical impedance spectroscopy (EIS) of the annealed LNMO coatings was conducted, and the results are depicted in Fig. 7. It is clear that EIS consists of two obvious semicircles in the high-to-medium frequency range and another straight line in the low frequency range. The EIS spectra and impedance data analysed on the basis of the equivalent circuit are shown in Fig. 7. The high frequency intercept at the real axis corresponds to the ohmic resistance (R_s) of the cell, mainly contributed by the electrode material, electrolyte, separator and contact resistance of the various parts.

The capacitive loop is caused by charge transfer resistance (R_{ct}). The straight line in the low frequency is the Warburg impedance (W) caused by the solid-phase diffusion in the electrode materials[21,22]. R_f and C_f represent the resistance and capacitance of the solid electrolyte interface (SEI), respectively[23,24]. It can be seen from Fig. 7 that the semicircle of the high frequency region and the medium frequency region increased significantly, as the cycle number increased from 1 to 20. This outcome suggests that the LNMO coating has a dynamic deterioration process and resistance to Li^+ migration increases after many cycles. It can be deduced that the sharp fading of capacity for the LNMO coating could be related to the interfacial side reaction between the surface of the active material and liquid electrolyte during the cycling process after 20 cycles, resulting in the continued growth of the undesired SEI layer functioning as a resistive layer for ionic conduction.

Electrochemical performance parameters of LNMO and annealed LNMO coatings show in table 2. LNMO has obvious redox peak at 4.6v / 4.8v, with higher capacity at 0.05c, 0.1c and 0.2c, respectively 100mAh/g, 80mAh/g and 78mAh/g.The performance of the annealed LNMO coatings samples is not as good as the original LNMO. But the fabrication of composite cathode electrodes by a binder-free deposition method and deposition methods such as APS are more efficient, making it is easier to fabricate LNMO coatings because these processes tend to sputter molten oxide compounds on the target body. This sputtering enables precise control of the thickness and a high deposition rate. As a consequence, grain refinement and enhancement of the density result in coatings with a higher physical strength using APS.

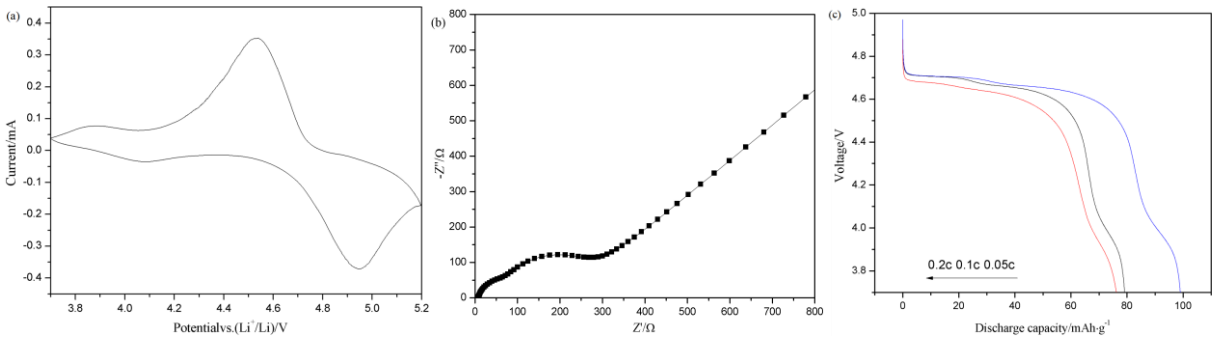

Figure 8.(a)Cyclic voltammetry of LNMO,(b)Electrochemical impedance spectroscopy (EIS) of LNMO,(c)Discharge curves of LNMO at various rates

Table 2. Electrochemical performance parameters of LNMO and annealed LNMO coatings

Electrochemical performance parameters	LNMO	annealed LNMO coatings
Oxidation peak(V)	4.6	2.75
Reduction peak(V)	4.8	3.25
$R_s(\Omega)$	53	55
$R_t(\Omega)$	76	123
$R_{ct}(\Omega)$	295	561
Discharge capacity of 0.05C($mAh \cdot g^{-1}$)	100	15.6
Discharge capacity of 0.1C($mAh \cdot g^{-1}$)	80	3.1
Discharge capacity of 0.2C($mAh \cdot g^{-1}$)	78	0.3

4. CONCLUSIONS

1) In this work, $LiNi_{0.5}Mn_{1.5}O_4$ powder was prepared by a sol-gel auto-combustion method, while $LiNi_{0.5}Mn_{1.5}O_4$ (LNMO) coatings were prepared by an atmospheric plasma spray (APS) method as a cathode electrode for lithium-ion batteries and have different electrochemical behaviour at 55℃ and 25℃.

2) The LNMO coatings exhibit the ordered cubic structure (space group $P4_332$), where the lattice constants of the annealed and un-annealed samples were 0.8176 nm and 0.8178 nm, respectively. The annealed LNMO coating exhibited well crystallized grains with an average size of approximately 1-4 μm.

3) The LNMO coating prepared by APS has better electrochemical cycle performance and rates performance at 55℃ than those at 25℃. EIS data results showed that the LNMO coating has a dynamic optimization process and resistance to Li^+ migration increases after 20 cycles.

4) The performance of the annealed LNMO coatings samples is not as good as the original LNMO. But the fabrication of composite cathode electrodes by a binder-free deposition method and deposition methods such as APS are more efficient.

ACKNOWLEDGEMENTS
This work was supported by Fund and Opening Project of Guangxi Key Laboratory of Automobile Components and Vehicle Technology, Guangxi University of Science and Technology (No.15-A-03-01,2015KFZD02); Innovation Project of GuangXi University of Science and Technology Graduate Education (YCSW2017200); Innovation Project of GuangXi University of Science and Technology Graduate Education (YCSW2018202);Science and Technology Cooperation Project of Guangzhou City (Grant No.201508030001).

References

1. Y. C. Wang, S. X. Zha, P. Y. Zha, F. Li, C. W. Nan, *J. Alloys Compd.*, 614(2014)271.
2. J.M. Chen, C.L. Tsai, C.Y. Yao, S. P. Sheu, H. C. Shih, *Mater. Chem. Phys.*, 51(1997)190.
3. C. K. Yang, L. Y. Qi, Z. Zuo, R. U. Wang, M. Ye, J. Ye, J. Lu, H. H. Zhou, *J. Power Sources*, 331(2016)487.
4. P. Kalyani, N. Kalaiselvi, N. G. Renganathan, M. Raghavan. *Mater. Res. Bull.*, 39(2004) 41.
5. B. Wang, W. A. Abdulla, D. Wang, X. S. Zhao, *Energ. Environ. Sci.*, 8(2015) 869.
6. Y. Wu, J. T. Zhang, C. B. Cao, S. Khalid, Q. Zhao, R. Wang, F. K. Butt, *Electrochim. Acta*, (2017)293.
7. H. C. Le, N. N. Dinh, S. Brutti, B. Scrosati, *Electrochim. Acta*, 55(2010)5110.
8. Q. Zhong, A. Bonakdarpour, M. Zhang, Y. Gao, J. R. Dahn, *J. Electrochem. Soc.*, 144(1997)205.
9. Yasushi. Idemoto, H. Narai, N. Koura, *J. Power Sources*, 119(2003)125.
10. Y. Li, Y. J. Gu, Y. B. Chen, H. Q. Liu, J. X. Ding, Y. M. Wang, *Mater. Lett.*, 180(2016) 105.
11. Y. S. Lee, Y. K. Sun, S. Ota, T. Miyashita, M. Yoshio, *Electrochem. Commun.*, 4(2002)989.
12. T. F. Yi, J. Mei, Y. R. Zhu, *J. Power Sources*, 316(2016)85.
13. M. Satyanarayana, Joseph. James, U.V. Varadaraju, *Appl. Surf Sci.*, 16(2004)906.
14. R. Amin, I. Belharouk, *J. Power Sources*, 348(2017)311.
15. J. Kotlan, R. C. Seshadri, S. Sampath, P. Ctibor, *Ceram. Int.*, 42(2016)11010.
16. K. Yang, J. Rong, J. W. Feng, Y, Zhuang, S. Y. Tao, C. X. Ding, *J. Eur. Ceram. Soc.*,

36(2016)4261.
17. D. Li, A. Ito, K. Kobayakawa, H. Noguchi, Y. Sato. *Electrochim. Acta*, 52(2007)1919.
18. Y. Idemoto, H. Narai, N. Koura. *J. Power Sources*, 125(2003)119.
19. G. Q. Liu, L. Wen, Y. M. Liu, *J. Solid State Electr.*, 14(2010)2191.
20. Y. C. Jin, C. Y. Lin, J. G. Duh, *Electrochim. Acta*, 69(2012)45.
21. X. Y. Zhou, J. J. Tang, J. Yang, Y. I. Zou, S. C. Wang, J. Xie, L. I. Ma. *Electrochim. Acta*, 70(2012)296.
22. X. Zhou, Y. Zou, J. Yang, *J. Solid State Chemistry*, 198(2013)231.
23. N. Zhang, T. Yang, L. Ye, K. Sun. *J. Alloys Compd.*, 509(2011)3783.
24. D. Aurbach, B. Markovsky, Y. Talyossef, G. Salitra, H. J. Kim, S. Choi. *J. Power Sources*, 162(2006)780.

© 2019 The Authors. Published by ESG (www.electrochemsci.org). This article is an open access article distributed under the terms and conditions of the Creative Commons Attribution license (http://creativecommons.org/licenses/by/4.0/).